Giant electrocaloric effect in ferroelectric ultrathin films at room temperature mediated by flexoelectric effect and work function

Ye Qiu, Huaping Wu, Jie Wang, Jia Lou, Zheng Zhang, Aiping Liu, Takayuki Kitamura, and Guozhong Chai

Citation: Journal of Applied Physics **122**, 024103 (2017); doi: 10.1063/1.4992811
View online: http://dx.doi.org/10.1063/1.4992811
View Table of Contents: http://aip.scitation.org/toc/jap/122/2
Published by the American Institute of Physics

Giant electrocaloric effect in ferroelectric ultrathin films at room temperature mediated by flexoelectric effect and work function

Ye Qiu,[1] Huaping Wu,[1,2,a)] Jie Wang,[3] Jia Lou,[4] Zheng Zhang,[1] Aiping Liu,[5] Takayuki Kitamura,[2] and Guozhong Chai[1,a)]
[1]*Key Laboratory of E&M, Zhejiang University of Technology, Ministry of Education and Zhejiang Province, Hangzhou 310014, China*
[2]*Department of Mechanical Engineering and Science, Kyoto University, Nishikyo-ku, Kyoto 615-8540, Japan*
[3]*Department of Engineering Mechanics, School of Aeronautics and Astronautics, Zhejiang University, Hangzhou 310027, China*
[4]*Piezoelectric Device Laboratory, Department of Mechanics and Engineering Science, Ningbo University, Ningbo, Zhejiang 315211, China*
[5]*Center for Optoelectronics Materials and Devices, Zhejiang Sci-Tech University, Hangzhou 310018, China*

(Received 28 March 2017; accepted 26 June 2017; published online 12 July 2017)

In ferroelectric ultrathin films, built-in electric fields are often present due to the flexoelectric effect and the difference of work functions at asymmetric electrodes, which may change the properties of the materials. In this paper, the influence of build-in electric fields induced by flexoelectric effect and/or work function difference on the misfit strain-temperature phase diagrams, and the electrocaloric properties of epitaxial $BaTiO_3$ ultrathin films are investigated by using an extended nonlinear thermodynamic theory. It is found that the flexoelectric effect, i.e., the coupling of polarization and strain gradient, changes the misfit strain-temperature phase diagrams notably, in which the phases with out-of-plane polarizations increase due to the presence of a built-in field. The electrocaloric properties are remarkably enhanced when the built-in fields induced by both the flexoelectric effect and work function difference are considered. In particular, a giant adiabatic temperature change of 7.89 K in ultrathin $Pt/BaTiO_3/SrRuO_3$ capacitors at 460 K is predicted. Moreover, it is demonstrated that the peak of adiabatic temperature change versus working temperature is shifted from a high temperature to room temperature, suggesting that ferroelectric ultrathin films with asymmetric electrodes and strain gradient are promising candidates for room temperature refrigeration. *Published by AIP Publishing*. [http://dx.doi.org/10.1063/1.4992811]

I. INTRODUCTION

The electrocaloric effect (ECE) is a reversible temperature change of a material upon the application or removal of an electric field under adiabatic conditions.[1–3] It may provide an efficient way to realize solid-state cooling devices for a broad range of applications such as on-chip cooling and temperature regulation for electronic devices. Refrigeration based on the ECE approach is more environmentally friendly than the existing vapor-compression approach.[4,5] The investigations on ECE have been increasing extensively since a giant ECE with an adiabatic temperature change of 12 K was found in $PbZr_{0.95}Ti_{0.05}O_3$ ferroelectric thin films by Mischenko *et al.*[6] Subsequently, several thin film ferroelectric systems such as relaxor ferroelectric films ($PbMg_{1/3}Nb_{2/3}O_3$-$PbTiO_3$),[7–9] ferroelectric polymer thin films [P(VDF-TrFE)](55/45),[10] and lead-free $SrBi_2Ta_2O_9$ (Ref. 11) thin films have also been confirmed to possess giant ECEs.

Recently, driven by the need for refrigeration device miniaturization and integration, many researches have focused on ferroelectric ultrathin films and tried to obtain a large ECE.[12–14] The definition of ferroelectric ultrathin films is still controversial. Generally speaking, the thickness of less than 10 nm is called a ferroelectric ultrathin film. For example, Liu *et al.*[12,13] have investigated the physical properties of ferroelectric ultrathin films whose thicknesses are less than 10 nm. Lu *et al.*[15] are interested in ferroelectric ultrathin films with thickness less than 6 nm. The ferroelectric ultrathin films exhibit different behaviors and properties from their bulk counterparts. One of the differences between ferroelectric ultrathin films and bulk materials is that the influence of built-in electric fields becomes more significant for the former. The built-in electric fields can be induced by the flexoelectric effect and the difference of work functions at asymmetric electrodes. Among different cases, the built-in electric field induced by the work function difference of asymmetric electrodes on ferroelectric ultrathin films has aroused growing interest in recent years.[16–18] When a ferroelectric ultrathin film is sandwiched between two dissimilar electrodes, the dissimilarity between two electrode/ferroelectric thin film interfaces introduces the asymmetry to the system.[19] It was pointed out as early as 1963 that different electronic and chemical environments of asymmetric electrode/ferroelectric thin film interfaces would induce a large electric field of electrode work function E_{bi} in ferroelectric thin films.[20] A previous study[13] shows that E_{bi} becomes significant in asymmetric capacitors and a giant ECE of 4.6 K at room temperature can be achieved in an asymmetric ultrathin $Pt/BaTiO_3$(BTO)/$SrRuO_3$(SRO) capacitor. Besides the difference of electrode work function, the flexoelectric effect

a)Authors to whom correspondence should be addressed: wuhuaping@gmail.com and chaigz@zjut.edu.cn

can also induce a large built-in electric field due to the presence of a large strain gradient in ferroelectric ultrathin films at the nanoscale. The flexoelectric effect describes a linear coupling between polarization and strain gradients.[21–23] The phenomenology of flexoelectric effect was firstly described by Kogan.[24] Then, a detailed theoretical study of flexoelectric effect in bulk crystals was performed by Tagantsev.[25,26] Experimental measurements of flexoelectric coefficient were carried out by Ma and Cross.[27–29] Renovation of the theoretical description for flexoelectric response of different nanostructures started from the papers of Catalan,[30,31] which has attracted the interest of many researchers. The built-in electric field induced by flexoelectric effect can also influence the ECE property. It was reported that an ECE of 1.5 K (at 289 K) was predicted from first-principles based simulations for $Ba_{0.5}Sr_{0.5}TiO_3$ (BST) under the application of a strain gradient of 1.5 μm^{-1},[32] in which the consideration of flexoelectric effect in the ferroelectric BST ultrathin film leads to an increase in adiabatic temperature change.

In order to obtain a large ECE, many articles have focused on influences of size effect, external electric field, and epitaxial strain on ferroelectric ultrathin films.[12,13,33] Nevertheless, the contribution of flexoelectric effect and difference of work function to ECE is relatively less considered. Moreover, a further analysis combining the effect of flexoelectric field and work function on the ECE in ferroelectric ultrathin films is still absent, which motivates us to further explore. In this article, we construct the effective energy expression of a single-domain ferroelectric ultrathin film with (001) orientation, in which the energies related to the flexoelectric effect and the electric field by difference of electrode work function are included. The misfit strain-temperature phase diagrams, polarization components, and ECE properties of the film are successfully analyzed and predicted by using the nonlinear Landau Devonshire theory. By carefully taking into account the influence of flexoelectric effect and work function, our studies reveal that phase diagrams and polarization components are changed dramatically, which enhances the electrocaloric (EC) properties of ferroelectric ultrathin films.

II. THERMODYNAMIC MODEL

The nonlinear Landau's thermodynamic theory can effectively describe and predict the phase transition behavior and physical properties of ferroelectrics.[34] We have investigated influences of strain on phase transition temperature and dielectric tenability of ferroelectric films,[35,36] which are well consistent with experimental results.[37,38] In addition, the theory has also been widely used in the theoretical study of the flexoelectric effect. We find that Catalan *et al.*[31] have investigated the effect of flexoelectricity on the dielectric properties of ferroelectric thin films, which is in good agreement with experimental measurements.[39] The nonlinear Landau Devonshire theory combined with mechanical boundary conditions is used to construct the effective energy expression of a ferroelectric ultrathin film including flexoelectric effect items. For an epitaxial (001) single-domain BTO ferroelectric ultrathin film grown on an $SrTiO_3$ substrate, the total energy expression of the Helmholtz free energy G_h can be deduced from the Gibbs free energy G_{gib} *via* the Legendre transformation[40,41]

$$G_h = G_{gib} + u_1\sigma_1 + u_2\sigma_2 + u_6\sigma_6, \tag{1}$$

where u_i and σ_i are the strain and stress of the BTO film. Meanwhile, we focus on the coupling flexoelectric effect between the polarization component P_3 along the film thickness (z direction) and the gradient of the in-plane direction (x direction) strain. Therefore, only the flexoelectric coefficient μ_{12} in the Gibbs energy expression is investigated. Thus, the expression for the elastic Gibbs free energy is presented as[42,43]

$$\begin{aligned}
G_{gib} = {} & a_1\left(P_1^2+P_2^2+P_3^2\right) + a_{11}\left(P_1^4+P_2^4+P_3^4\right) \\
& + a_{12}\left(P_1^2P_2^2+P_1^2P_3^2+P_2^2P_3^2\right) + a_{111}\left(P_1^6+P_2^6+P_3^6\right) \\
& + a_{112}\left[P_1^4\left(P_2^2+P_3^2\right)+P_3^4\left(P_1^2+P_2^2\right)+P_2^4\left(P_1^2+P_3^2\right)\right] \\
& + a_{123}P_1^2P_2^2P_3^2 + a_{1111}\left(P_1^8+P_2^8+P_3^8\right) \\
& + a_{1112}\left[P_1^6\left(P_2^2+P_3^2\right)+P_2^6\left(P_1^2+P_3^2\right)+P_3^6\left(P_1^2+P_2^2\right)\right] \\
& + a_{1122}\left(P_1^4P_3^4+P_2^4P_3^4+P_2^4P_1^4\right) \\
& + a_{1123}\left(P_1^4P_2^2P_3^2+P_1^2P_2^4P_3^2+P_1^2P_2^2P_3^4\right) \\
& - \frac{1}{2}s_{11}\left(\sigma_1^2+\sigma_2^2+\sigma_3^2\right) - s_{12}\left(\sigma_1\sigma_2+\sigma_1\sigma_3+\sigma_2\sigma_3\right) \\
& - \frac{1}{2}s_{44}\left(\sigma_4^2+\sigma_5^2+\sigma_6^2\right) - Q_{11}\left(\sigma_1P_1^2+\sigma_2P_2^2+\sigma_3P_3^2\right) \\
& - Q_{12}\left[\sigma_1\left(P_2^2+P_3^2\right)+\sigma_3\left(P_1^2+P_2^2\right)+\sigma_2\left(P_1^2+P_3^2\right)\right] \\
& - Q_{44}\left(P_2P_3\sigma_4+P_1P_3\sigma_5+P_2P_1\sigma_6\right) + \frac{1}{2}g_{11}\left(\frac{dP_3}{dz}\right)^2 \\
& + \frac{1}{2}\mu_{12}\left(\left(\sigma_1+\sigma_2\right)\frac{dP_3}{dz} - \left(\frac{d\sigma_1}{dz}+\frac{d\sigma_2}{dz}\right)P_3\right).
\end{aligned} \tag{2}$$

In this paper, considering that there is no vertical force on the surface of the film, so the film is in an approximately in-plane stress state ($\sigma_3 = \sigma_4 = \sigma_5 = 0$). Meanwhile, the in-plane misfit strain between the film and substrate is assumed as $u_1 = u_2 = u$, $u_6 = 0$. In view of the presence of a stress gradient in Eq. (2), strain is defined via the variational derivation

$$\frac{\partial G_{gib}}{\partial \sigma_i} - \frac{d}{dz}\left(\frac{\partial G_{gib}}{\partial \sigma_i'}\right) = -u. \tag{3}$$

Thus, we can obtain σ_i as follows:

$$\begin{aligned}
\sigma_1 = {} & \frac{\mu_{12}}{s_{11}+s_{12}}\frac{dP_3}{dz} + \frac{u}{s_{11}+s_{12}} \\
& - \frac{(s_{11}Q_{11}-s_{12}Q_{12})P_1^2 + (s_{11}Q_{12}-s_{12}Q_{11})P_2^2}{s_{11}^2-s_{12}^2} \\
& - \frac{Q_{12}}{s_{11}+s_{12}}P_3^2,
\end{aligned} \tag{4}$$

$$\sigma_2 = \frac{\mu_{12}}{s_{11}+s_{12}}\frac{dP_3}{dz} + \frac{u}{s_{11}+s_{12}} - \frac{(s_{11}Q_{12}-s_{12}Q_{11})P_1^2 + (s_{11}Q_{11}-s_{12}Q_{12})P_2^2}{s_{11}^2 - s_{12}^2} - \frac{Q_{12}}{s_{11}+s_{12}}P_3^2, \tag{5}$$

$$\sigma_6 = -\frac{Q_{44}P_1P_2}{s_{44}}. \tag{6}$$

According to Eqs. (4)–(6), the Helmholtz free energy G_h can be further expressed as

$$\begin{aligned} G_h = {} & a_1^*\left(P_1^2+P_2^2\right) + a_3^*P_3^2 + a_{11}^*\left(P_1^4+P_2^4\right) + a_{33}^*P_3^4 \\ & + a_{13}^*\left(P_1^2P_3^2+P_2^2P_3^2\right) + a_{12}^*P_1^2P_2^2 + a_{111}\left(P_1^6+P_2^6+P_3^6\right) \\ & + a_{112}\left[P_1^4\left(P_2^2+P_3^2\right) + P_2^4\left(P_1^2+P_3^2\right) + P_3^4\left(P_1^2+P_2^2\right)\right] \\ & + a_{123}P_1^2P_2^2P_3^2 + a_{1111}\left(P_1^8+P_2^8+P_3^8\right) \\ & + a_{1112}\left[P_1^6\left(P_2^2+P_3^2\right) + P_2^6\left(P_1^2+P_3^2\right) + P_3^6\left(P_1^2+P_2^2\right)\right] \\ & + a_{1122}\left(P_1^4P_3^4 + P_2^4P_3^4 + P_2^4P_1^4\right) \\ & + a_{1123}\left(P_1^4P_2^2P_3^2 + P_1^2P_2^4P_3^2 + P_1^2P_2^2P_3^4\right) + \frac{u^2}{s_{11}+s_{12}} \\ & + \frac{Q_{12}\mu_{12}}{s_{11}+s_{12}}P_3^2\frac{dP_3}{dz} - \frac{\mu_{12}^2}{s_{11}+s_{12}}P_3\frac{d^2P_3}{dz^2} \\ & - \frac{\mu_{12}}{s_{11}+s_{12}}\frac{du}{dz}P_3 + \frac{\mu_{12}u}{s_{11}+s_{12}}\frac{dP_3}{dz} + \frac{1}{2}g_{11}\left(\frac{dP_3}{dz}\right)^2, \end{aligned} \tag{7}$$

where

$$a_1^* = a_1 - u\frac{Q_{11}+Q_{12}}{s_{11}+s_{12}}, \tag{8a}$$

$$a_3^* = a_1 - u\frac{2Q_{12}}{s_{11}+s_{12}}, \tag{8b}$$

$$a_{11}^* = a_{11} + \frac{1}{2}\frac{1}{s_{11}^2-s_{12}^2}\left[\left(Q_{11}^2+Q_{12}^2\right)s_{11} - 2Q_{11}Q_{12}s_{12}\right], \tag{8c}$$

$$a_{33}^* = a_{11} + \frac{Q_{12}^2}{s_{11}+s_{12}}, \tag{8d}$$

$$a_{12}^* = a_{12} - \frac{1}{s_{11}^2-s_{12}^2}\left[\left(Q_{11}^2+Q_{12}^2\right)s_{12} - 2Q_{11}Q_{12}s_{11}\right] + \frac{Q_{44}^2}{2s_{44}}, \tag{8e}$$

$$a_{13}^* = a_{12} + \frac{Q_{12}(Q_{11}+Q_{12})}{s_{11}+s_{12}}, \tag{8f}$$

$$a_1 = \frac{T-T_0}{2\varepsilon_0 C}. \tag{8g}$$

Here, a_1, a_{ij}, a_{ijk}, and a_{ijkl} are the dielectric stiffness coefficients, P_i is polarization component, s_{ij} and Q_{ij} are the elastic compliances and electrostrictive coefficients, g_{11} and μ_{12} are gradient coefficient and flexoelectric coefficient, T_0 and C are the Curie–Weiss temperature and constant, and ε_0 is the permittivity of free space.

In addition, we concentrate on the 5 nm-thick BTO ultrathin film at the nanoscale; the polarization component along the film thickness is assumed to be homogenous. We can neglect the effect of the polarization gradient on the energy expression of Eq. (7). Thus, the final Helmholtz free energy can be further expressed as

$$\begin{aligned} G_h = {} & a_1^*\left(P_1^2+P_2^2\right) + a_3^*P_3^2 + a_{11}^*\left(P_1^4+P_2^4\right) + a_{33}^*P_3^4 \\ & + a_{13}^*\left(P_1^2P_3^2+P_2^2P_3^2\right) + a_{12}^*P_1^2P_2^2 \\ & + a_{111}\left(P_1^6+P_2^6+P_3^6\right) + a_{112}\left[P_1^4\left(P_2^2+P_3^2\right)\right. \\ & \left. + P_2^4\left(P_1^2+P_3^2\right) + P_3^4\left(P_1^2+P_2^2\right)\right] + a_{123}P_1^2P_2^2P_3^2 \\ & + a_{1111}\left(P_1^8+P_2^8+P_3^8\right) + a_{1112}\left[P_1^6\left(P_2^2+P_3^2\right)\right. \\ & \left. + P_2^6\left(P_1^2+P_3^2\right) + P_3^6\left(P_1^2+P_2^2\right)\right] + a_{1122}\left(P_1^4P_3^4\right. \\ & \left. + P_2^4P_3^4 + P_2^4P_1^4\right) + a_{1123}\left(P_1^4P_2^2P_3^2 + P_1^2P_2^4P_3^2\right. \\ & \left. + P_1^2P_2^2P_3^4\right) + \frac{u^2}{s_{11}+s_{12}} - \frac{\mu_{12}}{s_{11}+s_{12}}\frac{du}{dz}P_3. \end{aligned} \tag{9}$$

However, the depolarizing field and surface effect cannot be ignored. When the BTO film is sandwiched between top and bottom electrodes, the electric field energy can be determined as

$$G_{elec} = -P_iE_i - \frac{1}{2}E_{dep}P_3 - E_{bi}P_3, \tag{10}$$

where E_i is the applied electric field, E_{dep} is the depolarizing field, and E_{bi} is the work function field due to the difference between work function steps of ferroelectric-electrode 1 and ferroelectric-electrode 2 interfaces. The configurations are schematically shown in Fig. 1. E_{dep} and E_{bi} can be expressed as follows:[44,45]

$$E_{dep} = -\frac{\lambda_1+\lambda_2}{h\varepsilon_0 + (\lambda_1+\lambda_2)\varepsilon_b}P_3, \tag{11}$$

$$E_{bi} = -\frac{\Delta\varphi_2 - \Delta\varphi_1}{h} = -\frac{\varphi}{h}, \tag{12}$$

where h is the thickness of the BTO film, λ_i is the effective screening length of the interface, ε_b is the background dielectric constant, $\Delta\varphi_i$ is the work function step for the ferroelectric electrode i interface, and φ is the difference between work function steps. For a ferroelectric thin film at nanoscale, it is necessary to consider the surface energy which contains contributions of the near interface variation of polarization and the direct coupling between polarizations and interfaces. Note that the surface energy can be expressed as[44,45]

$$G_{surf} = (\zeta_1 - \zeta_2)P_i + \frac{1}{2}(\eta_1+\eta_2)P_i^2, \tag{13}$$

where ζ_i and η_i are the first order and second order coefficients of the surface energy G_{surf} expansion for the two

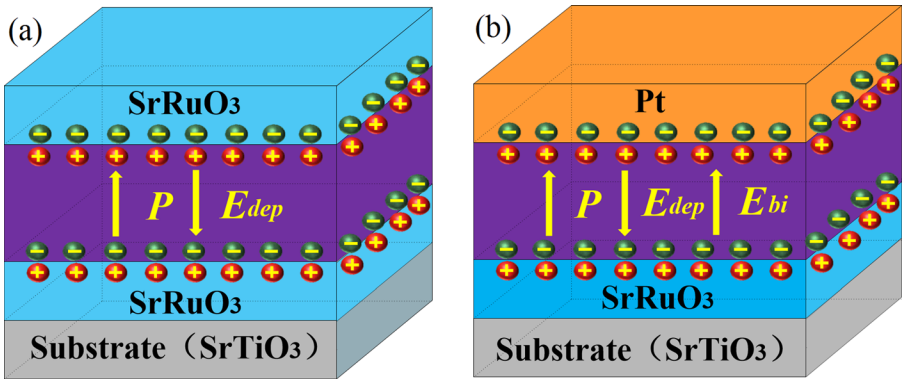

FIG. 1. Schematic configurations of the BTO ultrathin film with different electrodes: the arrows denote directions of spontaneous polarization P, depolarization field E_d, and work function field E_{bi}: (a) BTO with SRO and SRO symmetric electrodes and (b) BTO with Pt and SRO asymmetric electrodes.

ferroelectric electrode interfaces. The total effective energy expression of ferroelectric thin films can be given as

$$G = \int (G_h + G_{elec}) dv + \int G_{surf} ds. \tag{14}$$

Meanwhile, the equilibrium polarization P_i can be derived from the condition of thermodynamic equilibrium: $\partial G/\partial P_i = 0$. Then, when the applied electric field varies uniformly along a polarization direction, the EC coefficient ρ can be obtained as follows: $\rho = \partial P_i/\partial T$.[46] In this work, we focus on the electrocaloric effect in the thickness direction of the thin films, in which the external electric field and the built-in field are along the thickness direction. Thus, the EC coefficient ρ can be expressed as

$$\rho = \frac{\partial P_3}{\partial T}. \tag{15}$$

The EC change in temperature upon application of an electric field can be determined by[46]

$$\Delta T = -\frac{T}{C_E} \int_{E_1}^{E_2} \left(\frac{\partial P_3}{\partial T} \right)_E dE_3, \tag{16}$$

where C_E is the heat capacity of BTO, $C_E = 2.53 \times 10^6 \mathrm{J\,kg/K}$.[12]

III. RESULTS AND DISCUSSION

First, we investigate the flexoelectric effect on the ferroelectric properties of the BTO ultrathin film. It should be noted that the flexoelectric coefficient and strain gradient are important factors. The flexoelectric coefficient is a constant. However, the strain gradient in films is closely related to the clamping condition of the substrate, the deposition temperature, and the heat treatment process.[47–50] Therefore, it would be more appropriate to change the strength of the flexoelectric effect by adjusting the strain gradient inside ultrathin films. The in-plane strain u within the film is a function of the distance x_3 away from the substrate interface due to strain relaxation. In particular, the strain field distribution in films can be written as[51]

$$u(z) = u_0 \exp(-k \cdot z), \tag{17}$$

where $u(z)$ is the in-plane strain in the ultrathin film, u_0 is the lattice mismatch strain between the substrate and film. k is the stress relaxation coefficient, which is irrelevant to temperature. In the previous study, the k of $Pb(Zr, Ti)O_3$ (PZT) ($4 \times 10^6\,\mathrm{m^{-1}}$) has been explored in experiments by Kim *et al.*[51] For the strain field distribution in the form of exponential, the variation of k is totally equivalent to the change of the strain gradient.

In the following, we consider values of flexoelectric coefficient that have been experimentally and theoretically investigated.[52–55] We select a moderate flexoelectric coefficient $\mu_{12} = 1.6 \times 10^{-9}\,\mathrm{m^3/C}$ which has been theoretically studied by first-principle calculations.[52] In addition, the flexoelectric coefficient remains unchanged in the following calculation. Meanwhile, the BTO ultrathin films at various values of strain gradient are calculated in order to more clearly understand the influence of the flexoelectric effect. All the parameters we used are listed in Refs. 12 and 56. The misfit strain-temperature phase diagrams of the 5 nm-thick BTO ultrathin film sandwiched between symmetric electrodes, i.e., SRO/BTO/SRO, with $k = 0 \times 10^6\,\mathrm{m^{-1}}$, $2 \times 10^6\,\mathrm{m^{-1}}$, $4 \times 10^6\,\mathrm{m^{-1}}$, and $8 \times 10^6\,\mathrm{m^{-1}}$, respectively, are calculated by minimizing the total effective energy of Eq. (14), which are shown in Fig. 2.

In the case of $k = 0\ \mathrm{m^{-1}}$ from Fig. 2(a), this phase diagram consists of four equilibrium phases: (1) paraelectric p-phase: $P_1 = P_2 = P_3 = 0$; (2) c-phase: $P_1 = P_2 = 0$, $P_3 \neq 0$; (3) aa-phase: $P_1 = P_2 \neq 0, P_3 = 0$; (4) r-phase: $P_1 = P_2 \neq 0, P_3 \neq 0$. It can be seen that the phase diagram of the BTO is consistent with the previous result.[19] Figures 2(b), 2(c), and 2(d) show the role of the flexoelectric effect in driving the evolution of phase diagrams. When k takes the value of nonzero, the phase of ferroelectric ultrathin films becomes dramatically different. Thus, it is necessary to redefine phases: (1) ferroelectric c_1-phase (mesostable phase): $P_1 = P_2 = 0, |P_{3+}| > |P_{3-}| \neq 0$; (2) dielectric c_2-phase: $P_1 = P_2 = P_{3-} = 0, |P_{3+}| \neq 0$; (3) dielectric c_3-phase: $P_1 = P_2 = P_{3+} = 0, |P_{3-}| \neq 0$;[19] (4) ferroelectric r_1-phase (mesostable phase): $P_1 = P_2 \neq 0, |P_{3+}| > |P_{3-}| \neq 0$; (5) ferroelectric r_2-phase: $P_1 = P_2 \neq 0, |P_{3+}| \neq 0$; (6) ferroelectric r_3-phase: $P_1 = P_2 \neq 0, |P_{3-}| \neq 0$. In order to explain the special characteristic of the abovementioned phases, we calculated the energy profile of different phases [see the inset of Fig. 2(d)]. We can see that the energy profile is the well-known symmetric double-well (c phase red curve) for

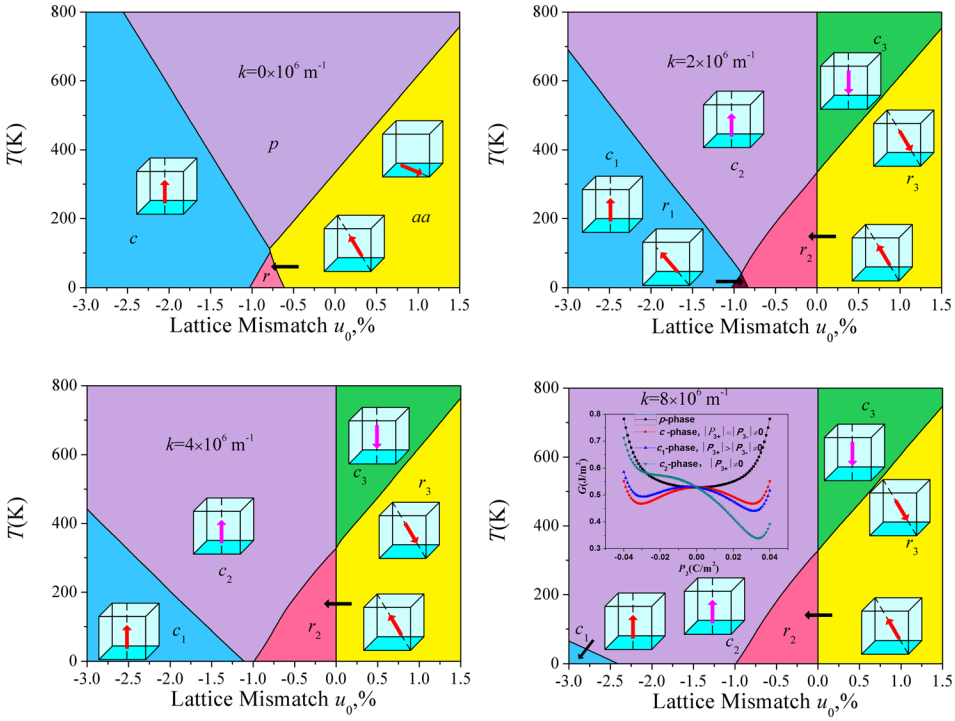

FIG. 2. Misfit strain-temperature phase diagram for the symmetric SRO/BTO/SRO capacitor when the stress relaxation coefficient is: (a) $k = 0 \times 10^6 \mathrm{m}^{-1}$, (b) $k = 2 \times 10^6 \mathrm{m}^{-1}$, (c) $k = 4 \times 10^6 \mathrm{m}^{-1}$, and (d) $k = 8 \times 10^6 \mathrm{m}^{-1}$. (The inset figure depicts the energy profile of different phases.)

ferroelectric films. Then, the energy profile turns to the asymmetric double-well (c_1 phase blue curve) due to the flexoelectric field. The energy curve has two non-equivalent local energy minima, indicating two non-equivalent polarization states. The positive flexoelectric field at this case results in an increase in the polarization component P_{3+},+leading to a c_1 phase state ($|P_{3+}| > |P_{3-}| \neq 0$).This asymmetric double-well is also proposed in a recent flexoelectric work based on theoretical and experimental studies.[57,58] Additionally, the energy profile that changes from the asymmetric double-well to single-well (c_2 phase green curve) induced by the increase of flexoelectric effect, indicates a transition from the ferroelectric phase to the dielectric phase.

Since we mainly analyze the coupling between the polarization P_3 and the in-plane strain gradient, the flexoelectric field along the thickness of the film is mainly considered. Therefore, according to $P_1 = P_2 = 0, P_3 \neq 0$, $\partial G/\partial P_3 = 0$, the governing equation that considers the flexoelectric effect along the z direction can be expressed as

$$(\eta_1 + \eta_2)P_3/h + 8a_{1111}P_3^7 + 6a_{111}P_3^5 + 4a_{33}^*P_3^3 + 2a_3^*P_3 = \frac{2\mu_{12}}{s_{11}+s_{12}}\frac{\partial u}{\partial z} + E_3 + E_{dep} + E_{bi}. \quad (18)$$

We can clearly see that the flexoelectric field E_{flexo} is $\frac{2\mu_{12}}{s_{11}+s_{12}}\frac{\partial u}{\partial z}$. Obviously, the numerical value of the flexoelectric field is proportional to the flexoelectric coefficient and the strain gradient of the ultrathin film, and the direction is determined by the two factors together. Moreover, the flexoelectric coefficient we used in the calculation is positive. Therefore, the positive flexoelectric field leads to an increase in the polarization component P_{3+} when the strain is compressive. From Figs. 2(a) and 2(b), it can be seen that the *c*-phase and the *r*-phase are replaced by the c_1-phase and the r_1-phase. At the same time, the c_2-phase and the r_2-phase can be found in the original region of the *p*-phase and the *aa*-phase. In contrast, the polarization component P_{3-} gradually increases because of the negative flexoelectric field in the region of tensile strain. Consequently, the c_3-phase and the r_3-phase can be found in the original region of the *p*-phase and the *aa*-phase. Compared with Figs. 2(b) and 2(c), there is a transition from the r_1-phase to the r_2-phase as a result of the enhancement of the polarization component P_{3+} induced by the increase of flexoelectric effect. Additionally, the energy profile that changes from the symmetric double-well shape to the asymmetric single-well shape indicates a transition from the c_1-phase to the c_2-phase. Furthermore, Fig. 2(d) shows that increasing k from $4 \times 10^6\,\mathrm{m}^{-1}$ to $8 \times 10^6\,\mathrm{m}^{-1}$ causes an expansion of the c_2-phase region.

The analysis of the above results suggests that the flexoelectric effect will change the polarization state of films. In order to further explain flexoelectric effect on ferroelectric ultrathin films, we plot the curves of polarization component with the lattice mismatch strain of ultrathin films under different strain gradients in Fig. 3. It can be clearly seen that the compressive strain is beneficial to the formation of P_3, and the tensile strain can lead to the decrease of P_3 and promote the formation of P_1, P_2, as depicted in Fig. 3(a). Compared with Figs. 3(a) and 3(b), the positive flexoelectric effect along the direction of the film thickness exists here, while the polarization component P_{3+} increased in the region of compressive strain. Meanwhile, the polarization component P_{3-} is found to be increased in the region of tensile strain. This is caused by the fact that the effect of the negative flexoelectric effect is stronger than the crystal lattice mismatch strain on polarization components. In addition, the enhancement of flexoelectric effect can lead to an increase in polarization component P_3. Specifically, comparing these results presented in Fig. 3, the original P_3 is $0.30\,\mathrm{C/m}^2$ for a SRO/BTO/SRO capacitor with a 5 nm-thick BTO ultrathin film at room temperature when misfit

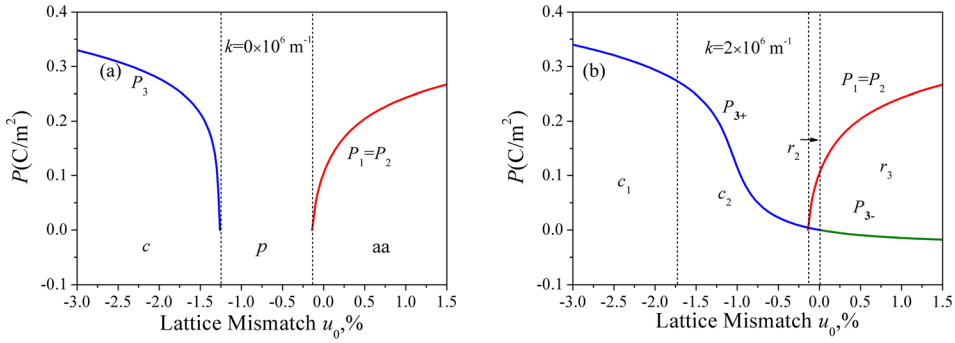

FIG. 3. Polarization component P as a function of the lattice mismatch strain for the symmetric SRO/BTO/SRO capacitor when the stress relaxation coefficient (a) $k = 0 \times 10^6 \mathrm{m}^{-1}$, (b) $k = 2 \times 10^6 \mathrm{m}^{-1}$, (c) $k = 4 \times 10^6 \mathrm{m}^{-1}$, and (d) $k = 8 \times 10^6 \mathrm{m}^{-1}$ at 298 K.

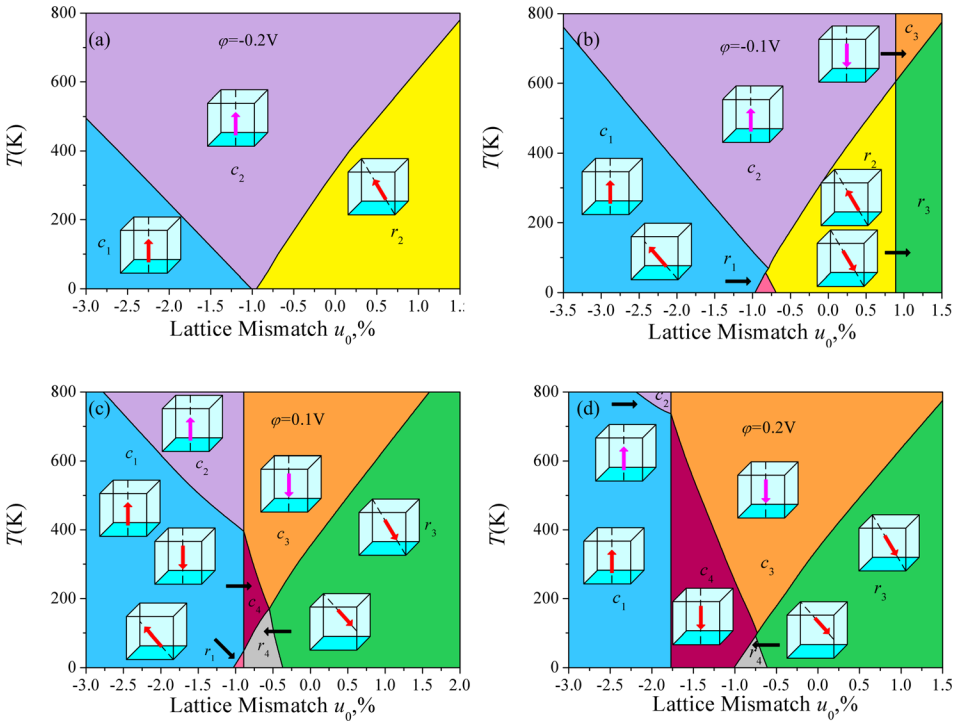

FIG. 4. Misfit strain-temperature phase diagram for the asymmetric Pt/BTO/SRO capacitor when the work function difference is: (a) $\varphi = -0.2$V, (b) $\varphi = -0.1$V, (c) $\varphi = 0.1$V, and (d) $\varphi = 0.2$V with the stress relaxation coefficient $k = 4 \times 10^6 \mathrm{m}^{-1}$.

strain $u_0 = -0.0246$. Moreover, since flexoelectric effect is taken into account, it is clearly observed that P_3 is 0.34 C/m^2 at the same conditions. It should be pointed out that the strain gradient is 96 432 m^{-1} at this moment. Nevertheless, it is easy to get the ferroelectric ultrathin film with the strain gradient of 10^5–10^6 in the experiment.[47] Thus, our study can provide a theoretical guideline for experiments. In brief, the flexoelectric effect is helpful in increasing polarizations, which is in good agreement with previous results.[59]

Second, we also investigate the influence of work function on the misfit strain-temperature phase diagrams of the asymmetric capacitors. When the BTO ultrathin film is sandwiched between dissimilar electrodes, i.e., Pt/BTO/SRO, the work function step difference φ leads to the formation of a work function electric field. The work function step is closely related to the material of electrodes and the clamping condition of electrodes. Meanwhile, the work function step values can be obtained through the first principle calculation.[44,45] The misfit strain-temperature phase diagrams of the 5 nm-thick BTO ultrathin film sandwiched between dissimilar electrodes, i.e., Pt/BTO/SRO, with $\varphi = -0.2$ V, -0.1 V, 0.1 V, and 0.2 V are calculated and shown in Fig. 4. Note that φ is the work function difference between the Pt and SRO electrodes.

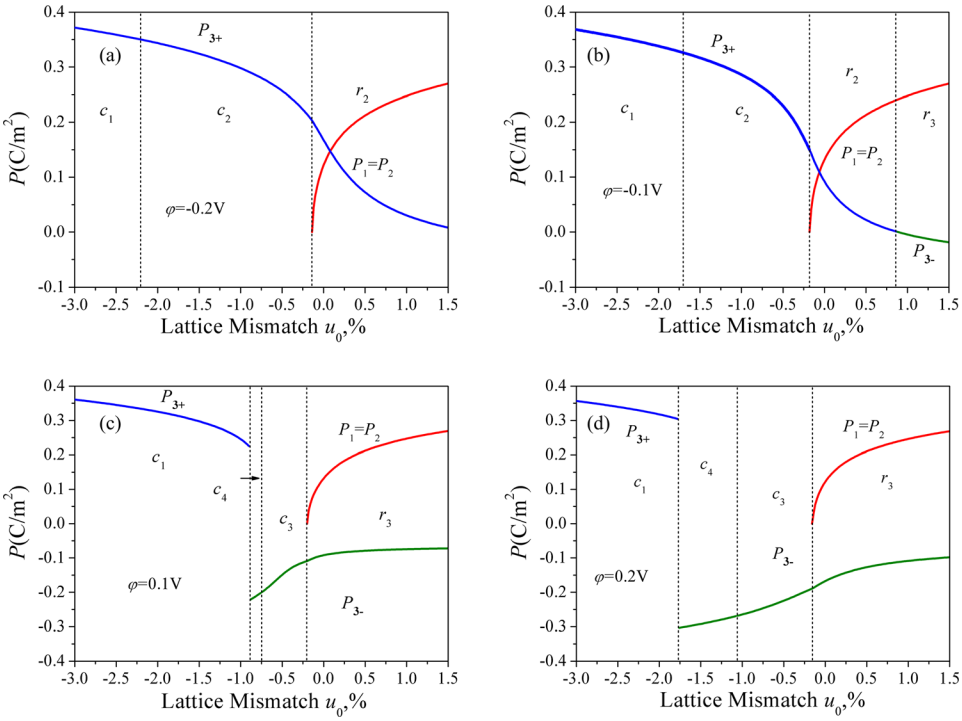

FIG. 5. Polarization component P as a function of the lattice mismatch strain for the asymmetric Pt/BTO/SRO capacitor when the work function difference is: (a) $\varphi = -0.2$V, (b) $\varphi = -0.1$V, (c) $\varphi = 0.1$V, and (d) $\varphi = 0.2$V at 298 K.

The E_{flexo} and E_{bi} are all considered as built-in electric fields in this paper. The E_{bi} is only related to the electrode work function difference and the film thickness. Besides, the value of E_{bi} is not related to the strain states of films. In the case of $\varphi = -0.2$ V and -0.1 V from Figs. 4(a) and 4(b), this can be deduced from Eq. (12) that the negative electrode work function difference will form the positive work function electric field E_{bi} in the film. However, the flexoelectric field is positive when the lattice mismatch strain is the compress strain. At the same time, the negative flexoelectric field corresponds to the tensile strain. As a consequence, the value of the built-in electric field is the sum of two electric fields in the region of compress strain. On the contrary, the value of built-in electric field is the subtraction of the two electric fields in the region of tensile strain. Figure 4(a) displays the phase diagram that consists of c_1-phase, c_2-phase, and r_2-phase, indicating that the main polarization component is P_{3+} during the application of a positive built-in electric field. As shown in Fig. 4(b), E_{bi} decreases as the magnitude of φ increases. Therefore, the total built-in electric field decreases in the region of compress strain so that the c_1-phase region expands and the c_2-phase region shrinks. Meanwhile, it is clear that the r_1-phase is formed in Fig. 4(b). Besides, the negative value of the total built-in electric field causes transitions from c_2-phase, r_2-phase to c_3-phase, and r_3-phase in the region of tensile strain. In the case of $\varphi = 0.1$ V and 0.2 V from Figs. 4(c) and 4(d), it can be seen that the work function electric field is negative, leads to the formation of a new c_4-phase (mesostable phase $P_1 = P_2 = 0, |P_{3-}| > |P_{3+}| \neq 0$) and r_4-phase (mesostable phase $P_1 = P_2 \neq 0, |P_{3-}| > |P_{3+}| \neq 0$) in the phase diagrams. This work function electric field could play a main role in the corresponding region.

Furthermore, the effect of the work function on the polarization components is shown in Fig. 5. It is found that the P_{3+} totally switches to the P_{3-}. Generally speaking, the polarization component of ferroelectric ultrathin films will switch under the external electric field or the mechanical stress field. The condition for obtaining a stable domain switching by using the external force is applying the atomic force microscope probe on the surface of the film, and the maximum force value reaches about 3 μN. If this force is applied in the region of the radius of 5 nm, the film surface will generate a local pressure of about 38.2 GPa which is much larger than the critical value 20 GPa of the BTO film.[60] It is worth mentioning that the external electric field is used to obtain a stable domain switching; the magnitude order 10^6–10^7 V/m of the electric field on the thin film is usually required. However, when the film thickness is thin, the electric field of this magnitude order could cause the breakdown of the film. Thus, we conclude that we can adjust the strain gradient and the state of the top and bottom electrodes to obtain a stable 180° domain switching, which is consistent with previous simulation results.[61,62] Meanwhile, we can avoid the risk of the destruction of the film.

Finally, we combine the flexoelectric effect with the work function to study the influence on the EC properties of ferroelectric ultrathin films. It should be pointed out that the external electric field is 500 kV/cm and remains unchanged in the following calculation. Furthermore, the external electric field E is in the same order of magnitude with E_{flexo} and E_{bi}. What's more, the strength of the total electric field (E_{flexo}, E_{bi} and external electric field E) will affect the sensitivity of polarization components due to the change of temperature. Specifically, the sensitivity is increased due to the decrease of the total electric field.[63] Interestingly, it is shown that two curves under the work function of 0.1 V and 0.4 V overlap well in Fig. 6(a). Detailed calculation proves that the total electric field absolute values of two curves are 3.0×10^7 V/m at 300 K. The same values also appear at other temperatures. Thus, this result clearly demonstrates the effect of

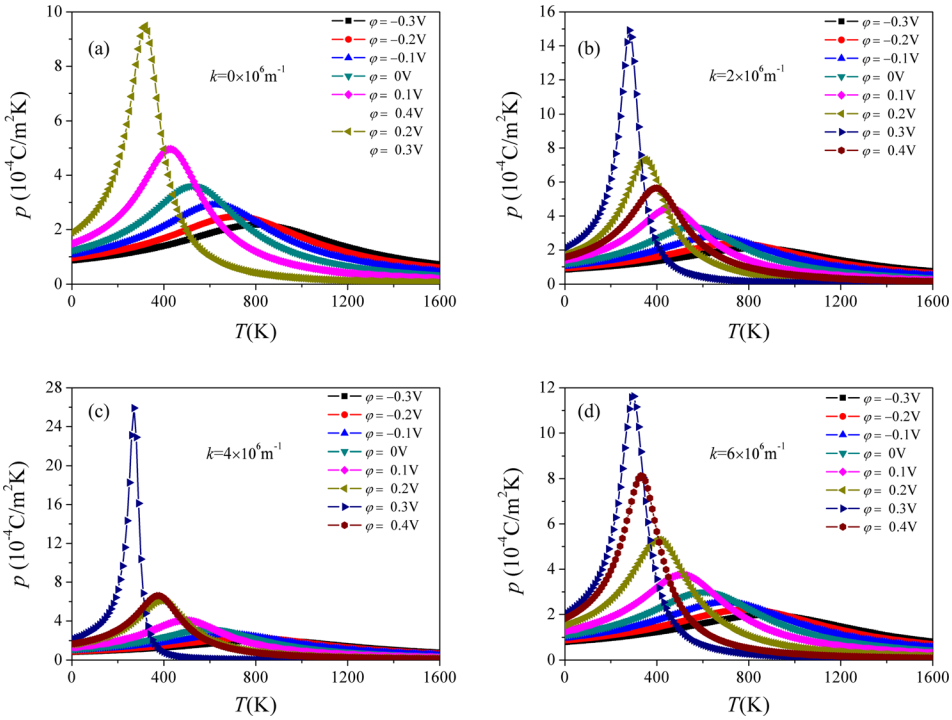

FIG. 6. EC coefficient p as a function of temperature T for the asymmetric Pt/BTO/SRO capacitor when the stress relaxation coefficient is: (a) $k = 0 \times 10^6 \mathrm{m}^{-1}$, (b) $k = 2 \times 10^6 \mathrm{m}^{-1}$, (c) $k = 4 \times 10^6 \mathrm{m}^{-1}$, and (d) $k = 6 \times 10^6 \mathrm{m}^{-1}$ with the applied electric field $E_3 = 500\,\mathrm{kV/cm}$ and the lattice mismatch strain $u_0 = -0.005$.

electric field on polarization sensitivity to temperature, which indicates that the electric field can be an effective tool to induce a large EC coefficient. Meanwhile, two curves under the work function of 0.2 V and 0.3 V are exactly the same. The reason is the same as above. Moreover, the EC coefficient is significantly enhanced under the positive difference of work function steps without considering the flexoelectric effect, as shown in Fig. 6(a). This result is caused by the decrease of the total electric field. Note that E_{bi} is negative at this moment according to Eq. (12), which is antiparallel to the direction of the external electric field. As expected, the EC coefficient changes relatively smoothly over the whole temperature range when the work function is negative. Overall, the peak value of the EC coefficient firstly increases as the magnitude of total electric field decreases. Then, the peak value of EC coefficient begins to decrease as the magnitude of total electric field increases. In the case of $\varphi = 0.2$ V and 0.3 V from Fig. 6(a), the value of total electric field is minimum, which causes the largest EC coefficient. This result agrees well with a recent work that shows the EC coefficient on SRO/BTO/SRO capacitors under different values of the external electric field.[12] Comparing these results presented in Fig. 6, it is seen that the maximum peak value of EC coefficient can be obtained when $k = 4 \times 10^6\,\mathrm{m}^{-1}$. This is because total electric field is minimum than other circumstances. Here, it becomes imperative to mention that the peak of EC coefficient is higher than that obtained without the flexoelectric effect. In particular, a maximum EC coefficient of 25.9 $\times 10^{-4}\mathrm{C/m^2\,K}$ (at 270 K) and a room temperature EC coefficient of 10.4 $\times 10^{-4}\mathrm{C/m^2K}$ (at 300 K) can be obtained. A comparison of the present results with those reported in the literature is given in Table I. The analysis of the result suggests that the flexoelectric effect and work function have a beneficial impact on the EC coefficient.

TABLE I. Pyroelectric coefficient of selected materials near room temperature.

Material	ρ ($10^{-4}\mathrm{C/m^2\,K}$)	Operating temperature (K)	References
$Bi_{0.5}Na_{0.5}TiO_3$	5.7	303	64
BTO	9.5	322.47	12
BTO	9.2	390	65
BTO	12	415	65
BST	14	300	21
BST	30	286	21
BTO	25.9	270	Present work
BTO	10.4	300	Present work
PZT	4.14	303	66
PVDF-TRFE	0.4	313	67

In addition to the EC coefficient ρ, the adiabatic temperature change ΔT is also an important parameter. Thus, we focus on the combined effect of flexoelectric effect and electrode work function on the ΔT. The ΔT–T curves of the 5 nm-thick BTO ultrathin film sandwiched between dissimilar electrodes, i.e., Pt/BTO/SRO, with $\varphi = -0.3$ V, -0.2 V, -0.1 V, 0 V, 0.1 V, 0.2 V, 0.3 V, and 0.4 V, $k = 0 \times 10^6\mathrm{m}^{-1}$, $2 \times 10^6\mathrm{m}^{-1}$, $4 \times 10^6\mathrm{m}^{-1}$, and $6 \times 10^6\mathrm{m}^{-1}$ are calculated and shown in Fig. 7. The peak value of ΔT is 7.77 K at 470 K under $\varphi = 0.1$ V, as shown in Fig. 7(a). Obviously, the negative E_{bi} is antiparallel with P_3, which induces a large polarization change. Thus, a significant enhancement of ΔT is observed. This result is in line with previous research.[13] Furthermore, an important feature found here is a remarkable shift of the ΔT peak from high temperature to room temperature, which is desired for cooling applications. These behaviors also exist in $k = 2 \times 10^6\mathrm{m}^{-1}$, $4 \times 10^6\mathrm{m}^{-1}$, and $6 \times 10^6\mathrm{m}^{-1}$ plotted in Figs. 7(b), 7(c), and 7(d). Moreover, due to the increase of the flexoelectric effect, the work function that the peak value of ΔT requires is heightened. For

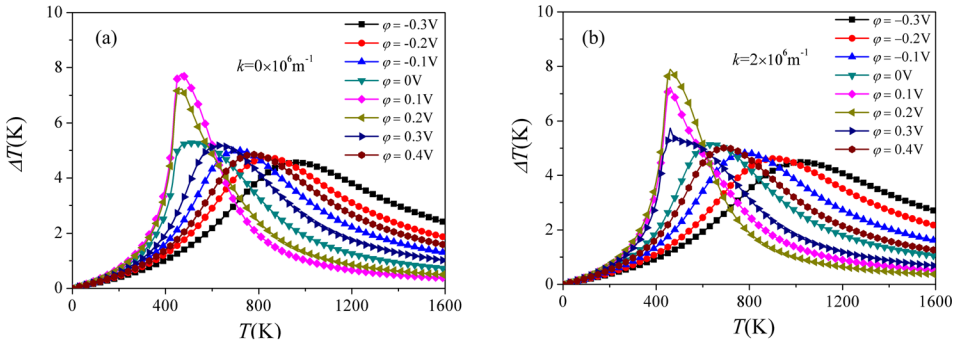

FIG. 7. Adiabatic temperature change ΔT as a function of temperature T for the asymmetric Pt/BTO/SRO capacitor when the stress relaxation coefficient is: (a) $k = 0 \times 10^6 \mathrm{m}^{-1}$, (b) $k = 2 \times 10^6 \mathrm{m}^{-1}$, (c) $k = 4 \times 10^6 \mathrm{m}^{-1}$, and (d) $k = 6 \times 10^6 \mathrm{m}^{-1}$ with the applied electric field $E_3 = 500\,\mathrm{kV/cm}$ and the lattice mismatch strain $u_0 = -0.01$.

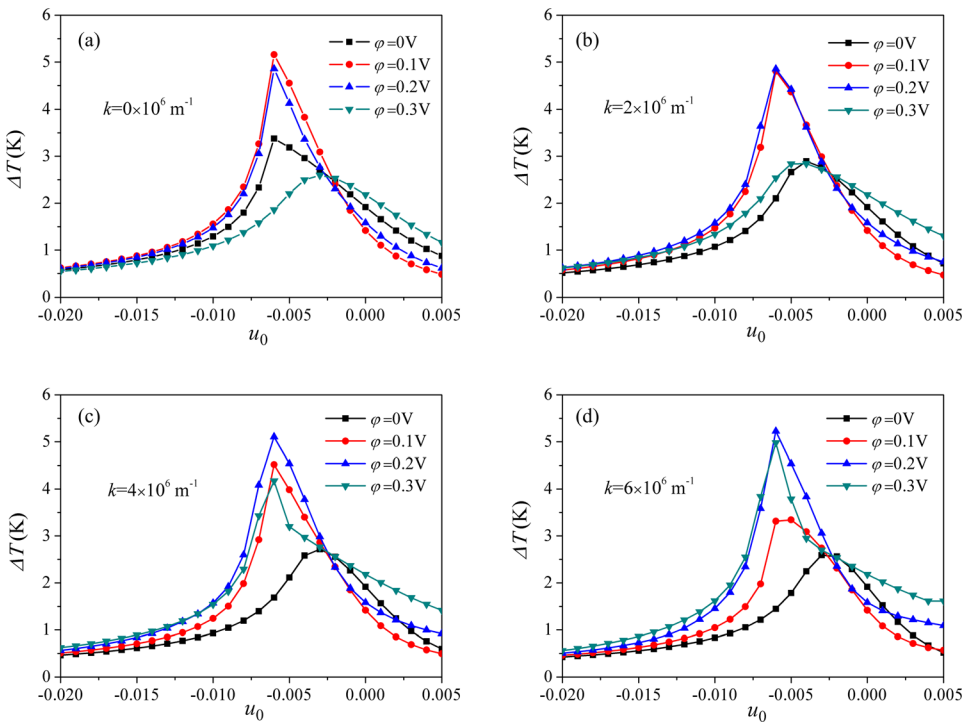

FIG. 8. Adiabatic temperature change ΔT as a function of the lattice mismatch strain for the asymmetric Pt/BTO/SRO capacitor when the stress relaxation coefficient is: (a) $k = 0 \times 10^6 \mathrm{m}^{-1}$, (b) $k = 2 \times 10^6 \mathrm{m}^{-1}$, (c) $k = 4 \times 10^6 \mathrm{m}^{-1}$, and (d) $k = 6 \times 10^6 \mathrm{m}^{-1}$ at 300 K with the applied electric field $E_3 = 500\,\mathrm{kV/cm}$.

practical cooling devices, it is of great importance to explore a kind of potential EC material which is environmentally friendly and works at room temperature. This may provide opportunities for exploring more practical application induced by flexoelectric effect and work function.

In order to meet the needs of practical use, we choose $T = 300\,\mathrm{K}$ to calculate the effect of the combination of flexoelectric effect and work function on ΔT. According to the above investigation, the peak value of ΔT is found to be increased under the influence of positive work function, indicating that the EC properties can be greatly tuned by designing the asymmetric electrode. Therefore, ΔT is calculated when $\varphi = 0\,\mathrm{V}$, 0.1 V, 0.2 V, and 0.3 V, shown in Fig. 8. The maximum peak value of ΔT is 5.22 K at 300 K under an electric field of 500 kV/cm, which is larger than most of the theoretical and experimental results in BTO-based samples near room temperature (Table II). For instance, 4.5 K in modified BTO ceramics ($\Delta E = 145\,\mathrm{kV/cm}$ at 312 K),[70] 2.5 K in the BTO ultrathin film ($\Delta E = 500\,\mathrm{kV/cm}$ at 300 K),[12] and 4.6 K in the BTO ultrathin film ($\Delta E = 12\,500\,\mathrm{kV/cm}$ at 300 K).[13] The result obtained in this work is larger than the largest one, i.e., 7.1 K reported in BTO multilayer capacitors

TABLE II. A comparative analysis of the various adiabatic temperature changes reported in the literature for BTO.

Samples	Form	T (K)	ΔT (K)	ΔE (kV/cm)	References
BTO	Single crystal	409	0.9	12	68
BTO	Ultrathin film	300	5.22	500	Present work
BTO	Ultrathin film	460	7.89	500	Present work
BTO	Ceramic	400	1.4	10	70
BTO	Ceramic MLC	353	7.1	800	71
BTO	Ultrathin film	300	5.8	12 500	13
BTO	Ultrathin film	300	4.6	12 500	13
BTO	Ultrathin film	300	3.5	12 500	13
BTO	Ceramic	312	4.5	145	70
BTO	Ultrathin film	300	2.5	500	12
BTO	MLC	303	1.3	176	69

(MLCs) ($\Delta E = 800\,\text{kV/cm}$ at 353 K).[71] Meanwhile, the position of the peak is concentrated in the region of compressive strain. It can be seen that the selected specific strain value is reasonable in Figs. 6 and 7. At the same time, the corresponding electrode work function of the peak value increases with the enhancement of the flexoelectric effect, which is in good agreement with the *p*-T curves in Fig. 7. Based on these results, it can be concluded that choosing the proper flexoelectric coefficient and the work function can make the film get a larger adiabatic temperature change at room temperature. The present findings imply that it is possible to consider the mutual effect of lattice mismatch strain, flexoelectric effect, and the work function, thereby leading to a new strategy to improve the EC properties. Most importantly, it may provide the practical guidance for designing the microrefrigerator based on the ferroelectric ultrathin films.

IV. CONCLUSIONS

In summary, we have investigated the influences of the flexoelectric effect and the work function on the phase diagrams, polarization components, and electrocaloric properties of epitaxial BTO ultrathin films using an extended thermodynamic model. It is found that the misfit strain-temperature phase diagrams can be significantly affected. Due to the built-in electric field induced by the flexoelectric effect and work function, the polarization along the electric field is remarkably enhanced. Moreover, a stable polarization switching under the condition of avoiding damaging films is displayed. The results demonstrate that the existence of flexoelectric effect and work function is helpful in increasing ΔT and EC coefficient. A giant ΔT of 7.89 K ($\Delta E = 500\,\text{kV/cm}$ at 460 K) and an EC coefficient of 25.9 $\times 10^{-4}\text{C/m}^2\text{K}$ ($\Delta E = 500\,\text{kV/cm}$ at 270 K) are reported. What is more, the peak of ΔT shows a shift to a room working temperature under a positive work function and flexoelectric field. More concretely, a ΔT of 5.22 K and an EC coefficient of 10.4 $\times 10^{-4}\text{C/m}^2\text{K}$ at room temperature can be achieved ($\Delta E = 500\,\text{kV/cm}$ at 300 K). Hence, appropriate tunability of the flexoelectric effect, work function, and lattice mismatch strain can reinforce the electrocaloric effect and improve the practical application at room temperature, which is extremely needed to develop cooling devices based on ferroelectric ultrathin films. We believe that our results will stimulate further work on making ferroelectric films to get a large adiabatic temperature change at room temperature. It may provide an efficient means to design refrigeration devices for practical applications.

ACKNOWLEDGMENTS

This work was supported by the National Science Foundation of China (Grant Nos. 11372280, 11672269, and 51675485) and the Zhejiang Provincial Natural Science Foundation of China (Grant No. LY16E020011).

[1]M. Valant, Prog. Mater. Sci. **57**, 980 (2012).
[2]X. Moya, S. Kar-Narayan, and N. D. Mathur, Nat. Mater. **13**, 439 (2014).
[3]A. Chanthbouala, A. Crassous, V. Garcia, K. Bouzehouane, S. Fusil, X. Moya, J. Allibe, B. Dlubak, J. Grollier, S. Xavier, C. Deranlot, A. Moshar, R. Proksch, N. D. Mathur, M. Bibes, and A. Barthelemy, Nat. Nanotechnol. **7**, 101 (2012).
[4]X. Dai, H.-X. Cao, Q. Jiang, and V. C. Lo, J. Appl. Phys. **106**, 034103 (2009).
[5]B. Li, J. B. Wang, X. L. Zhong, F. Wang, and Y. C. Zhou, J. Appl. Phys. **107**, 014109 (2010).
[6]A. S. Mischenko, Q. Zhang, J. F. Scott, R. W. Whatmore, and N. D. Mathur, Science **311**, 1270 (2006).
[7]A. S. Mischenko, Q. Zhang, R. W. Whatmore, J. F. Scott, and N. D. Mathur, Appl. Phys. Lett. **89**, 242912 (2006).
[8]T. M. Correia, J. S. Young, R. W. Whatmore, J. F. Scott, N. D. Mathur, and Q. Zhang, Appl. Phys. Lett. **95**, 182904 (2009).
[9]Z. Feng, D. Shi, R. Zeng, and S. Dou, Thin Solid Films **519**, 5433 (2011).
[10]B. Neese, B. Chu, S.-G. Lu, Y. Wang, E. Furman, and Q. M. Zhang, Science **321**, 821 (2008).
[11]H. Chen, T. L. Ren, X. M. Wu, Y. Yang, and L. T. Liu, Appl. Phys. Lett. **94**, 182902 (2009).
[12]Y. Liu, X. P. Peng, X. J. Lou, and H. Zhou, Appl. Phys. Lett. **100**, 192902 (2012).
[13]Y. Liu, I. C. Infante, X. J. Lou, and B. Dkhil, Appl. Phys. Lett. **104**, 082901 (2014).
[14]E. Glazkova, C. M. Chang, S. Lisenkov, B. K. Mani, and I. Ponomareva, Phys. Rev. B. **92**, 064101 (2015).
[15]X. Lu, H. Li, and W. Cao, J. Appl. Phys. **112**, 074115 (2012).
[16]C. J. Li, L. S. Huang, T. Li, W. M. Lu, X. P. Qiu, Z. Huang, Z. Q. Liu, S. W. Zeng, R. Guo, Y. L. Zhao, K. Y. Zeng, M. Coey, J. S. Chen, Ariando, and T. Venkatesan, Nano Lett. **15**, 2568 (2015).
[17]Y. Zheng, W. J. Chen, C. H. Woo, and B. A. Wang, J. Phys. D: Appl. Phys. **44**, 095401 (2011).
[18]R. Soni, A. Petraru, P. Meuffels, O. Vavra, M. Ziegler, S. K. Kim, D. S. Jeong, N. A. Pertsev, and H. Kohlstedt, Nat. Commun. **5**, 5414 (2014).
[19]W. J. Chen, Y. Zheng, B. Wang, D. C. Ma, and C. M. Wu, J. Appl. Phys. **115**, 094101 (2014).
[20]J. G. Simmons, Phys. Rev. Lett. **10**, 10 (1963).
[21]H. Zhou, Y. M. Pei, F. X. Li, H. S. Luo, and D. N. Fang, Appl. Phys. Lett. **104**, 061904 (2014).
[22]C. Liu, H. P. Wu, and J. Wang, Appl. Phys. Lett. **109**, 192901 (2016).
[23]M. S. Majdoub, P. Sharma, and T. Cagin, Phys. Rev. B **77**, 125424 (2008).
[24]S. M. Kogan, Sov. Phys. Solid State **5**, 2069 (1964).
[25]A. K. Tagantsev, Phys. Rev. B **34**, 5883 (1986).
[26]A. K. Tagantsev, Phase Transit. **35**, 119 (1991).
[27]W. H. Ma and L. E. Cross, Appl. Phys. Lett. **82**, 3293 (2003).
[28]W. Ma and L. E. Cross, Appl. Phys. Lett. **79**, 4420 (2001).
[29]W. H. Ma and L. E. Cross, Appl. Phys. Lett. **81**, 3440 (2002).
[30]G. Catalan, B. Noheda, J. McAneney, L. J. Sinnamon, and J. M. Gregg, Phys. Rev. B **72**, 020102 (2005).
[31]G. Catalan, L. J. Sinnamon, and J. M. Gregg, J. Phys.: Condens. Matter **16**, 2253 (2004).
[32]S. Patel, A. Chauhan, J. Cuozzo, S. Lisenkov, I. Ponomareva, and R. Vaish, Appl. Phys. Lett. **108**, 162901 (2016).
[33]A. Grunebohm, M. Marathe, and C. Ederer, Europhys. Lett. **115**, 47002 (2016).
[34]X. Lu, H. Li, and W. Cao, J. Appl. Phys. **114**, 224106 (2013).

[35]H. Wu, G. Chai, B. Xu, J. Li, and Z. Zhang, Appl. Phys. A **113**, 155 (2013).
[36]H. P. Wu, X. F. Ma, Z. Zhang, J. Zhu, J. Wang, and G. Z. Chai, J. Appl. Phys. **119**, 154102 (2016).
[37]S. A. Harrington, J. Y. Zhai, S. Denev, V. Gopalan, H. Y. Wang, Z. X. Bi, S. A. T. Redfern, S. H. Baek, C. W. Bark, C. B. Eom, Q. X. Jia, M. E. Vickers, and J. L. MacManus-Driscoll, Nat. Nanotechnol. **6**, 491 (2011).
[38]O. J. Lee, S. A. Harrington, A. Kursumovic, E. Defay, H. Y. Wang, Z. X. Bi, C.-F. Tsai, L. Yan, Q. X. Jia, and J. L. MacManus-Driscoll, Nano Lett. **12**, 4311 (2012).
[39]L. J. Sinnamon, M. M. Saad, R. M. Bowman, and J. M. Gregg, Appl. Phys. Lett. **81**, 703 (2002).
[40]N. A. Pertsev, A. G. Zembilgotov, and A. K. Tagantsev, Phys. Rev. Lett. **80**, 1988 (1998).
[41]N. A. Pertsev, V. G. Kukhar, H. Kohlstedt, and R. Waser, Phys. Rev. B **67**, 054107 (2003).
[42]A. N. Morozovska, E. A. Eliseev, M. D. Glinchuk, L. Q. Chen, and V. Gopalan, Phys. Rev. B **85**, 094107 (2012).
[43]A. K. Tagantsev, E. Courtens, and L. Arzel, Phys. Rev. B **64**, 224107 (2001).
[44]A. K. Tagantsev, G. Gerra, and N. Setter, Phys. Rev. B **77**, 174111 (2008).
[45]G. Gerra, A. K. Tagantsev, and N. Setter, Phys. Rev. Lett. **98**, 207601 (2007).
[46]G. Akcay, S. P. Alpay, G. A. Rossetti, and J. F. Scott, J. Appl. Phys. **103**, 024104 (2008).
[47]D. Lee, A. Yoon, S. Y. Jang, J. G. Yoon, J. S. Chung, M. Kim, J. F. Scott, and T. W. Noh, Phys. Rev. Lett. **107**, 057602 (2011).
[48]A. Gruverman, B. J. Rodriguez, A. I. Kingon, R. J. Nemanich, A. K. Tagantsev, J. S. Cross, and M. Tsukada, Appl. Phys. Lett. **83**, 728 (2003).
[49]D. Lee, B. C. Jeon, A. Yoon, Y. J. Shin, M. H. Lee, T. K. Song, S. D. Bu, M. Kim, J. S. Chung, J. G. Yoon, and T. W. Noh, Adv. Mater. **26**, 5005 (2014).
[50]D. Lee and T. W. Noh, Philos. Trans. R. Soc. A **370**, 4944 (2012).
[51]H. J. Kim, S. H. Oh, and H. M. Jang, Appl. Phys. Lett. **75**, 3195 (1999).
[52]T. Xu, J. Wang, T. Shimada, and T. Kitamura, J. Phys.: Condens. Matter **25**, 415901 (2013).
[53]J. W. Hong and D. Vanderbilt, Phys. Rev. B **88**, 174107 (2013).
[54]J. W. Hong and D. Vanderbilt, Phys. Rev. B **84**, 180101 (2011).
[55]W. H. Ma and L. E. Cross, Appl. Phys. Lett. **88**, 232902 (2006).
[56]Y. L. Li, L. E. Cross, and L. Q. Chen, J. Appl. Phys. **98**, 064101 (2005).
[57]H. Zhou, J. W. Hong, Y. H. Zhang, F. X. Li, Y. M. Pei, and D. N. Fang, Physica B. **407**, 3377 (2012).
[58]H. Lu, C. W. Bark, D. E. de los Ojos, J. Alcala, C. B. Eom, G. Catalan, and A. Gruverman, Science **336**, 59 (2012).
[59]G. Bai, K. Qin, Q. Xie, X. Yan, C. Gao, and Z. Liu, Mater. Lett. **186**, 146 (2017).
[60]Y. Gaillard, A. H. Macias, J. Munoz-Saldana, M. Anglada, and G. Trapaga, J. Phys. D: Appl. Phys. **42**, 085502 (2009).
[61]L. Jiang, Y. Zhou, Y. Zhang, Q. Yang, Y. Gu, and L.-Q. Chen, Acta Mater. **90**, 344 (2015).
[62]L. Jiang, J. Tang, Y. Zhou, Q. Yang, Y. Zhang, L. Guo, and X. Zhong, Comput. Mater. Sci. **108**, 309 (2015).
[63]J. Zhang, R. Xu, A. R. Damodaran, Z. H. Chen, and L. W. Martin, Phys. Rev. B **89**, 224101 (2014).
[64]F. Guo, B. Yang, S. Zhang, F. Wu, D. Liu, P. Hu, Y. Sun, D. Wang, and W. Cao, Appl. Phys. Lett. **103**, 182906 (2013).
[65]G. Akcay, S. P. Alpay, J. V. Mantese, and G. A. Rossetti, Appl. Phys. Lett. **90**, 252909 (2007).
[66]S. T. Lau, C. H. Cheng, S. H. Choy, D. M. Lin, K. W. Kwok, and H. L. W. Chan, J. Appl. Phys. **103**, 104105 (2008).
[67]B. Ploss, B. Ploss, F. G. Shin, H. L. W. Chan, and C. L. Choy, IEEE Trans. Dielectr. Electr. Insul. **7**, 517 (2000).
[68]X. Moya, E. Stern-Taulats, S. Crossley, D. Gonzalez-Alonso, S. Kar-Narayan, A. Planes, L. Manosa, and N. D. Mathur, Adv. Mater. **25**, 1360 (2013).
[69]Y. Bai, G. P. Zheng, and S. Q. Shi, Appl. Phys. Lett. **96**, 192902 (2010).
[70]Y. Bai, X. Han, X. C. Zheng, and L. J. Qiao, Sci. Rep. **3**, 2895 (2013).
[71]Y. Bai, G. P. Zheng, K. Ding, L. J. Qiao, S. Q. Shi, and D. Guo, J. Appl. Phys. **110**, 094103 (2011).